X-ray diffraction for phase identification in Ti-based alloys: benefits and limitations

Physica Scripta

PAPER

X-ray diffraction for phase identification in Ti-based alloys: benefits and limitations

L Bolzoni and F Yang

School of Engineering, The University of Waikato, Hamilton 3240, New Zealand

E-mail: bolzoni.leandro@gmail.com

Keywords: titanium alloys, x-ray diffraction, microstructure, phases, equilibrium

OPEN ACCESS

RECEIVED
29 December 2023

REVISED
25 March 2024

ACCEPTED FOR PUBLICATION
3 May 2024

PUBLISHED
14 May 2024

Abstract

X-ray diffraction (XRD) is routinely used to characterise Ti alloys, as it provides insight on structure-related aspects. However, there are no dedicated reports on its accuracy are available. To fill this gap, this work aims at examining the benefits and limitations of XRD analysis for phase identification in Ti-based alloys. It is worth mentioning that this study analyses both standard and experimental Ti alloys but the scope is primarily on alloys slow cooled from high temperature, thus characterised by equilibrium microstructures. To be comprehensive, this study considers the all spectrum of Ti alloys, ranging from alpha to beta Ti alloys. It is found that successful identification and quantification of the phases is achieved in the majority of the different type of Ti-based alloys. However, in some instances like for near-alpha alloys, the output of XRD analysis needs to be complemented with other characterisation techniques such as microscopy to be able to fully characterise the material. The correlation between the results of XRD analysis and the molybdenum equivalent parameter (*MoE*), which is widely used to design Ti alloys, was also investigated using structural-analytical models. The parallel model is found to be the best to estimate the amount of β-Ti phase as a function of the *MoE* parameter.

1. Introduction

Materials characterisation techniques are paramount when developing advanced materials. Amongst them, x-ray diffraction (XRD) is a simple, powerful, non-destructive method used on both particulate and bulk materials [1]. XRD is commonly used as able to provide basic information about the structure/phases [2], texture [3] as well as other more advanced structural parameters including crystallinity, lattice strain [4], and crystal defects [5]. The output of a XRD experiment is a XRD pattern in which the position and relative intensity of the peaks yield the fingerprint of the underlying crystalline structure. This is used to identify the phases present in the material, derived the unit cells, and identify the diffraction planes of such unit cells [6]. This is possible because an incident x-rays beam with an angle θ is reflected off with the same angle. Such reflection derives from crystal planes that are a distance d apart. The Bragg law (i.e. $\lambda = 2d \sin\theta$, where λ is the wavelength) is then used to deduce the crystal structure based on the constructive interfere between the incident and reflected beams [1]. Comparing and contrasting experimental XRD patterns with databases permits to label the diffraction peaks present in the material.

Titanium (Ti) and its alloys are advanced materials generally used in high demanding applications like aerospace/aeronautic and biomedical because of the wide range of combinations of properties they provide [7–9]. Such combinations of performance are achievable because Ti is an allotropic material. The addition of alloying elements either stabilises the low temperature hexagonal close packed (HCP) α-Ti phase or the high temperature body centred cubic (BCC) β-Ti phase, with some few exceptions [10, 11]. Ti alloys are, therefore, categorised as α alloys, $\alpha+\beta$ Ti alloys, and β alloys depending on the dominant phase(s) present in the microstructure [12, 13]. Nevertheless, the addition of specific alloying elements, the use of particular processing procedure, or the combination of both can also bring about the formation of metastable phases in Ti.

Table 1. Composition and type of Ti-based alloys analysed.

Composition	Alloy type	Status	References
Pure Ti	Alpha (α)	Standard	[19]
Ti-3Al-2.5 V	Near-alpha (α)	Standard	[20]
Ti-1Cu-1Mn	Near-alpha (α)	Experimental	[21]
Ti-6Al-4V	Alpha+beta ($\alpha+\beta$)	Standard	[22]
Ti-2Nb-2Fe	Alpha+beta ($\alpha+\beta$)	Experimental	[23]
Ti-5Al-5V-5Mo-3Cr	Near-beta (β)	Standard	[24]
Ti-5Mn-5Nb	Near-beta (β)	Experimental	[25]
Ti-5Mn-5Fe	Metastable beta (β)	Experimental	[26]
Ti-10Mn	Stable beta (β)	Experimental	[27]

Specifically, α', α", athermal ω, and isothermal ω are the main metastable phases that can be formed in Ti [14]. More in detail, the hexagonal α'martensitic phase is commonly obtained upon quenching of Ti alloys with low-to-medium amount of β stabilisers. As the α'martensitic phase shares the same lattice and Burger orientation relationships with the β-Ti phase of the α-Ti phase (i.e. $(110)_\beta//(0002)_\alpha$ and $[1\,\bar{1}\,1]_\beta//[11\,\bar{2}\,0)_\alpha$), it is generally difficult to discern them purely based on XRD measurements. With the increment of the amount of β stabilisers, the lattice of the α'martensitic phase gets distorted, losing the hexagonal symmetry, and thus transforming into the orthorhombic α" martensitic phase. The two types of ω phase share the same trigonal/non-compact hexagonal lattice, depending on whether the amount of β stabilisers is very high or high, respectively. However, the athermal one forms upon the decomposition of the β-Ti phase in alloys where the martensitic transformation is suppressed whereas the isothermal one forms during ageing heat treatments. It is worth mentioning that all these non-equilibrium phases (i.e. α', α", athermal ω and isothermal ω) generally lead to the embrittlement of the alloy [15]. Thus they are generally avoided or used either as transient phases upon subsequent heat treatments (i.e. quenching plus ageing [16, 17]) or to enhance a specific property (e.g. stiffness [18]).

To the best knowledge of the authors, there is not a specific dedicated piece of work in literature analysing the accuracy of XRD for detecting phases in Ti alloys with near-equilibrium microstructure. This will be valuable as XRD is universally employed when new Ti alloys with unprecedented compositions are developed. Therefore, this work aims to highlight the advantages and limitations of using XRD for the characterisation of the phases present in different types of Ti-based alloys. These include alpha, alpha+beta, and beta Ti alloys, covering the full spectrum of Ti alloys. Furthermore, the work is complemented with the establishment of the correlation between the output of XRD analysis and the molybdenum equivalent parameter (*MoE*). This is significant as the *MoE* parameter is routinely used to design new Ti alloys.

2. Alloys analysed

A variety of Ti-based alloys were considered to analyse the advantages and limitations of XRD to identify the phase(s) constituting them. The composition and type of Ti-based alloys analysed are reported in table 1. It is worth mentioning that compositions are in weight percentage (wt%), unless otherwise indicated. For the sake of comparison and make to study more reliable, both standard and experimental Ti alloys were considered. A standard Ti alloy is an established material utilised in industry and that can be found in handbooks like [10], whereas experimental Ti alloys are new alloys being created for enhanced performance or reduced cost.

The Ti-based alloy compositions of table 1 were obtained through powder metallurgy, which generally involves shaping of the loose powder and its consolidation via sintering. The selected Ti-based alloys, whose manufacturing details can be found in the specific references, were slow cooled, resulting in a near-equilibrium microstructure. The only exception is the Ti-10Mn alloy, which was forged in the β field (i.e. 1150 °C) [27].

XRD patterns of the Ti-based alloys were obtained by means of Philips X'pert with Cu K_α radiation (1.54 Å). For that the materials were scanned at a rate of 0.013°, with dwell time of 0.5 s, in the 30–80° range. In order to confirm the phases present in the near-equilibrium microstructure of the Ti-based alloys, the samples were cut and prepared metallographically using progressively finer SiC grinding papers followed by polishing using an OPS solution. A water-based Kroll solution ($2HF + 4HNO_3$, vol.%) was eventually used to chemically etch the samples to reveal the microconstituents. Microstructural analysis was performed via an Olympus BX-60 optical microscope and a Hitachi S-4700 SEM equipped with an EDS detector.

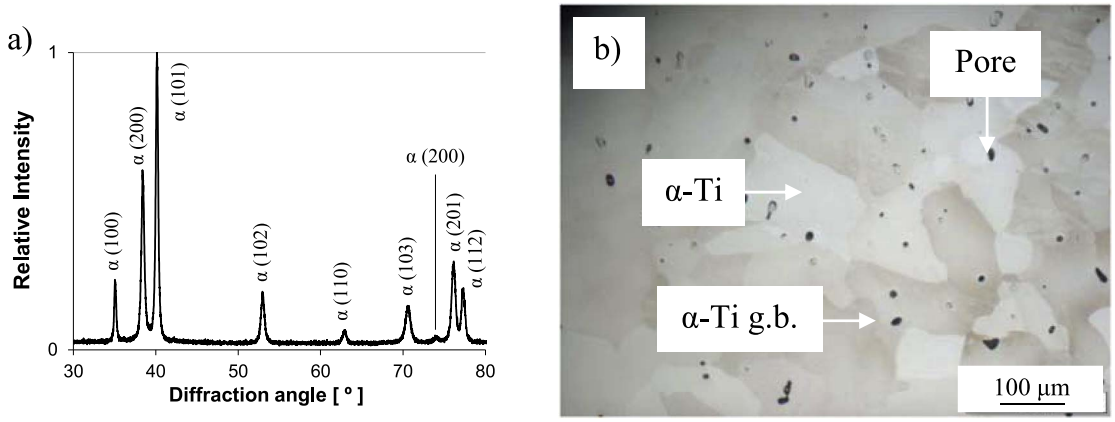

Figure 1. XRD pattern of pure Ti (a) and associated optical micrograph (b).

3. XRD and microstructural analyses

Figure 1 shows the XRD pattern of pure Ti and the associated optical micrograph. As expected, only diffraction peaks related to the α-Ti phase are present in the XRD pattern (figure 1(a)). This XRD pattern is the typical of pure Ti slow cooled from above its beta transus. Upon colling, α-Ti grains nucleate and grow from the prior β-Ti that constitute the material at high temperatures. Due to the slow cooling characteristic of vacuum sintering, which results in a near-equilibrium microstructure, the α-Ti (101) plane peak has the highest relative intensity. A similar behaviour is also found in pure Ti processed via repeated cold-rolling and annealing steps as demonstrated by the study of Niu *et al* [28] where the material is characterized by equiaxed grains and the α-Ti (101) plane peak is the major XRD peak. In agreement with the XRD results, the microstructure of pure Ti is entirely composed of equiaxed α-Ti grains (figure 1(b)). It is worth mentioning that, as the alloys were obtained through powder metallurgy, residual pores are present in the microstructure. They are visible as isolated, (almost)spherical, black dots in the micrograph. They are found either at the α-Ti grain boundaries (i.e. α-Ti g.b.) or inside the α-Ti grains.

The XRD patterns of the standard (Ti-3Al-2.5 V) and experimental (Ti-1Cu-1Mn) near-alpha Ti alloys analysed are presented in figure 2. As for pure Ti, only diffraction peaks related to the α-Ti phase are present in the XRD patterns. No significant differences can be highlighted depending on the nature of alloy, if not minor variations in the relative intensity of the diffraction peaks detected. The α-Ti (101) plane peak is still the one with the highest relative intensity. The positions of possible β-Ti phase diffraction peaks are superimposed (blue dotted lines) in the experimental XRD patterns (figure 2(a)). This clearly shows that no β-Ti phase was detected whatsoever, not even as an overlapping peak. This could have been the case between the α-Ti (101) plane peak and the peak of the β-Ti (100) family-planes. The absence of peaks related to the β-Ti phase in near-alpha Ti alloys is common in literature regardless of the processing route used. For example, Yu *et al* [29] found such behaviour in the Ti-6.5Al-2Sn-3Zr-1.5Mo-1.5Nb-0.4Si-0.2Y-0.4 C alloy obtained via either casting or hot isostatic pressing, this is also the case when processing the Ti-3Al-2.5 V alloy by means of vacuum hot-pressing [30].

The analysis of the microstructure of the standard (figure 2(b)) and experimental (figure 2(c)) near-alpha Ti alloys shows the classical lamellar microstructure. Such structure is constituted of α-Ti grain boundaries and alternating parallel lamellae of α-Ti and β-Ti phases. In these optical micrographs, the α-Ti phase is visible as the bright phase and the β-Ti phase as the dark one. Even though there are differences in terms of size of the grains and width of the lamellae, the β-Ti phase is obviously present. The stabilisation of the β-Ti phase is due to the addition of β stabilisers, namely V, Cu and Nb in this instance. The differences in terms of the microstructural phases' features are related to the type, amount, and relative stabilisation strength of the individual alloying elements. Specifically, Al is an α stabiliser and, therefore, decreases the stability of the β-Ti phase. In terms of relative stabilisation strength, Cu is the strongest, followed by V and Nb as per the *MoE* definitions [31–33]. Consequently, the standard Ti-3Al-2.5 V alloy has an overall coarser microstructure with respect to the experimental Ti-1Cu-1Mn alloy. Analysis of the standard Ti-3Al-2.5 V alloy via SEM-EDS yielded an average chemical composition of 95.4Ti-3.6Al-1.0 V and 91.3Ti-2.8Al-5.9 V for α-Ti and β-Ti, respectively. For the experimental Ti-1Cu-1Mn alloys, the α-Ti and β-Ti phases were, respectively, found to be 98.8Ti-0.7Cu-0.5Mn and 95.7Ti-2.3Cu-2.0Mn.

Figure 3 shows the XRD patterns of the standard (Ti-6Al-4V) and experimental (Ti-2Nb-2Fe) alpha+beta Ti alloys and their optical micrographs. Conversely to near-alpha Ti alloys (figure 2(a)), diffraction peaks related to

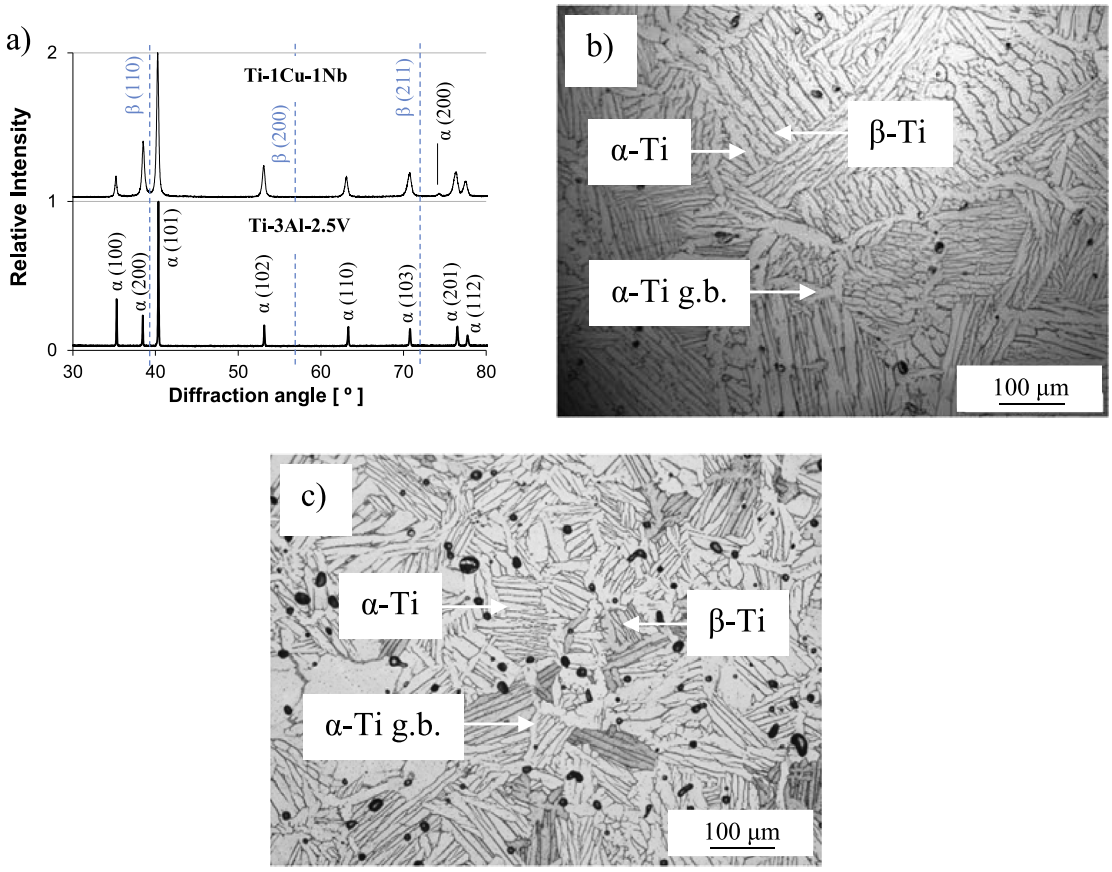

Figure 2. XRD patterns of the near-alpha Ti alloys (a) and associated optical micrographs: (b) Ti-3Al-2.5 V (standard), and (c) Ti-1Cu-1Mn (experimental).

both the α-Ti and β-Ti phases were detected. The α-Ti phase is still the predominant as the diffraction peak of the α-Ti (101) plane is the one with the strongest relative intensity. The type and relative intensity of the β-Ti phase' peaks vary depending on the chemistry of the alloy as it is strictly correlated with the amount of stabilised β-Ti phase (figure 3(a)). On the one side, the β-Ti (100) family-planes' peak is the only β-Ti phase' peak detected for the standard Ti-6Al-4V alloy. On the other side, peaks of the β-Ti (100), (200), and (211) family of planes were detected for the experimental Ti-2Nb-2Fe alloy. This trend is common in alpha+beta Ti alloys and peaks of the β-Ti phase can also be detected in the Ti-6Al-4V alloy manufactured using hot extrusion as demonstrated by the study of Luo *et al* [34] when aiming to achieve a dual harmonic structure.

Both the Ti-6Al-4V (figure 3(b)) and Ti-2Nb-2Fe (figure 3(c)) alloys are characterised by a lamellar microstructure composed of equiaxed α-Ti grains filled with $\alpha+\beta$ lamellae. As for near-alpha Ti alloys (figure 2), the features of the microconstituents of the lamellar structure are remarkable different depending on the nature of the alloy. The Ti-2Nb-2Fe alloy has a significantly finer microstructure than the Ti-6Al-4V alloy. This is due to the fact that the latter alloy bears Al as α stabiliser in its composition and Fe is a much stronger β stabiliser in comparison to V [31–33]. Consequently, a considerable much greater amount of β-Ti phase is stabilised upon slow cooling of the Ti-2Nb-2Fe alloy compared to the Ti-6Al-4V alloy. This, in turn, justifies the detection of different β-Ti phase' peaks with higher relative intensity in the experimental Ti-2Nb-2Fe alloy (figure 3(a)). From EDS analysis, the Ti-6Al-4V alloy is composed of 92.2Ti-6.3Al-1.5 V (α-Ti) and 81.7Ti-7.2Al-11.1 V (β-Ti), and the Ti-2Nb-2Fe alloy by 97.5Ti-1.6Nb-0.9Fe (α-Ti) and 91.9Ti-2.7Nb-6.5Fe (β-Ti).

The XRD patterns of the standard (Ti-5Al-5V-5Mo-3Cr) and experimental (Ti-5Mn-5Nb) near-beta Ti alloys analysed are shown in figure 4. As for previously analysed alpha+beta Ti alloys, diffraction peaks of the α-Ti and β-Ti phases were found in the XRD patterns. The influence of the chemistry of the alloy is also clear. Therefore, the β-Ti (100) family-planes' peak is the one with the greatest relative intensity in the case of the Ti-5Al-5V-5Mo-3Cr alloy, indicating that the β-Ti phase is the predominant in the material. Conversely, in the case of the Ti-5Mn-5Nb alloy it is the α-Ti (101) plane that has the highest relative intensity. Consistently, the relative intensity of the other diffraction peaks of the β-Ti phase (i.e. 200 and 211) is also higher in the case of the Ti-5Al-5V-5Mo-3Cr alloy. It is worth mentioning that metastable phases can form in near-beta Ti alloys, especially when cooled under non-equilibrium conditions. However, no diffraction peaks of any metastable

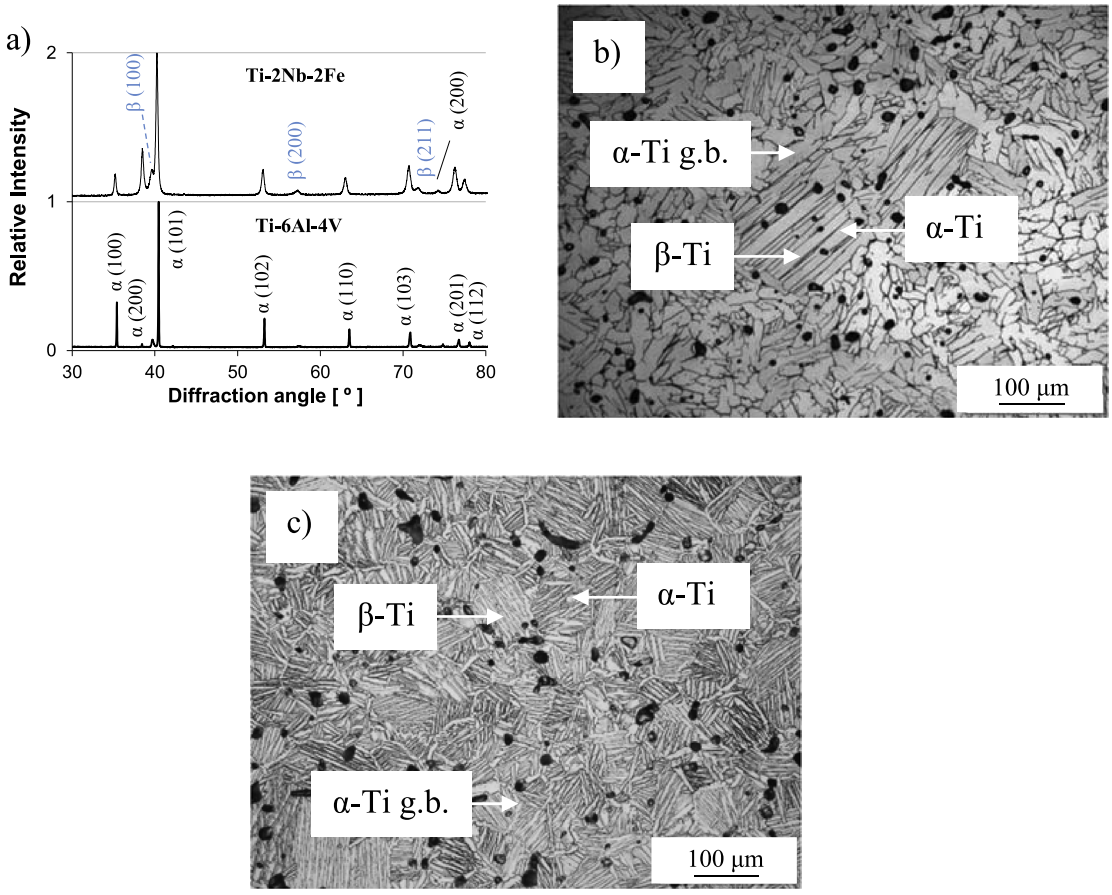

Figure 3. XRD patterns of the alpha+beta Ti alloys (a) and associated optical micrographs: (b) Ti-6Al-4V (standard), and (c) Ti-2Nb-2Fe (experimental).

phase were detected confirming that such phases did not form upon slow cooling from the sintering temperature. Such behaviour is proven in the near-beta Ti-5Al-5V-5Mo-3Cr alloy processed by selective laser melting [35] where only peaks of the β-Ti phase were detected as a consequence of the high solidification rate.

Figure 4 also shows that the standard Ti-5Al-5V-5Mo-3Cr and experimental Ti-5Mn-5Nb near-beta Ti alloys are both characterised by a lamellar microstructure. The phases constituting the structure are the same, but their relative amount and distribution is different. Specifically, the $\alpha+\beta$ lamellae are found within equiaxed β-Ti grains in the Ti-5Al-5V-5Mo-3Cr alloy (figure 4(b)) whereas they are confined by α-Ti grain boundaries in the case of the Ti-5Mn-5Nb alloy (figure 4(c)). This is in agreement with the results of the XRD analysis where the β-Ti (100) family-planes' peak was the predominant in the XRD pattern of the Ti-5Al-5V-5Mo-3Cr alloy. It is worth noting that in the micrographs of figure 4 the colours of the phases of the two alloys are inverted. In particular, the β-Ti phase appears as dark in the micrograph of the Ti-5Mn-5Nb alloy whilst it is the bright phase in the micrograph of the Ti-5Al-5V-5Mo-3Cr alloy. The resulting average EDS chemical composition for the α-Ti and β-Ti phases are, respectively, 93.4Ti-2.5Al-1.6Mo-1.5C-1.0Cr and 84.6Ti-2.5Al-4.8Mo-5.1C-3.0Cr for the Ti-5Al-5V-5Mo-3Cr alloy, and 89.2Ti-2.4Mn-3.1 Nb and 82.8Ti-9.5Mn-7.7 Nb for the Ti-5Mn-5Nb alloy.

Figure 5 shows the XRD patterns of the experimental metastable beta (Ti-5Mn-5Fe) and stable beta (Ti-10Mn) Ti alloys and the relative optical micrographs. For both alloys, the diffraction peak with the highest relative intensity is that of the β-Ti (100) family of planes. However, in the case of the Ti-5Mn-5Fe alloys, due to its metastable nature, diffraction peaks of the α-Ti phase are also present. Contrarywise, only diffraction peaks of the β-Ti phase were found for the Ti-10Mn alloy. Coherently, Wang *et al* [36] found a comparable behaviour where the microstructure is composed of equiaxed β-Ti grains and only β-Ti phase XRD peaks are detected in their proposed new biomedical Ti-Mn-Nb alloys subjected to a solution treatment.

The micrographs of the metastable beta Ti-5Mn-5Fe (figure 5(b)) and stable beta Ti-10Mn (figure 5(c)) alloys shows that both materials are characterised by a structure composed of equiaxed β-Ti grains. Nevertheless, grains of the α-Ti phase with acicular or needle-like morphology are also present in the microstructure of the Ti-5Mn-5Fe alloys, which is not the case for the Ti-10Mn alloy. The phases found in the microstructure are, therefore, consistent with the results of the XRD analysis. The precipitation of the acicular α-Ti grains is related to the total amount of alloying elements added and their β-Ti phase stabilisation strength.

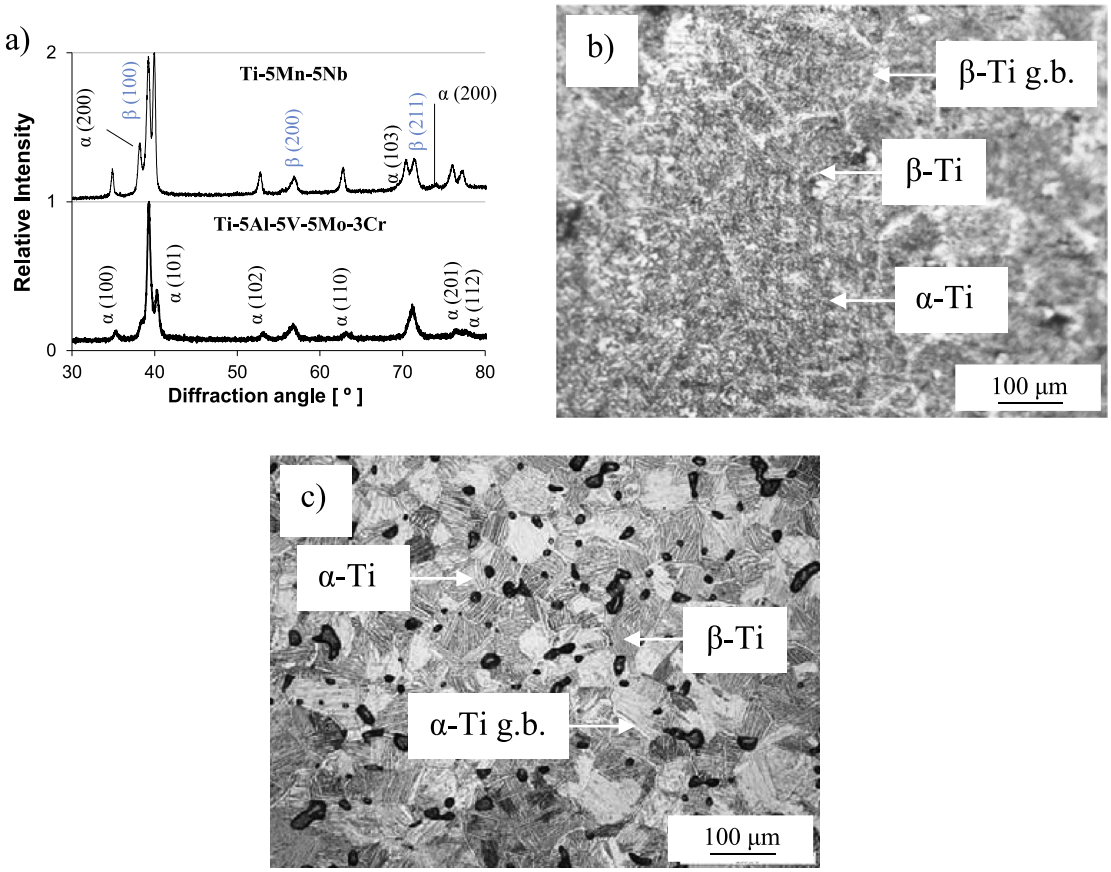

Figure 4. XRD patterns of the near-beta Ti alloys (a) and associated optical micrographs: (b) Ti-5Al-5V-5Mo-3Cr (standard), and (c) Ti-5Mn-5Nb (experimental).

This determines the metastable/stable nature of each specific Ti alloy and whether suppression of the α-Ti $\rightarrow$ β-Ti allotropic phase transformation and full stabilisation of the β-Ti phase is achieved. However, the manufacturing route used to process the alloy has also an impact. In particular, the Ti-10Mn alloy analysed was processed via forging in the β field (i.e. 1150 °C) [27], where the higher cooling rate of open die forging, with respect to vacuum sintering, contributed to the suppression of the precipitation of the α-Ti phase.

4. Discussion

XRD is a simple, powerful, non-destructive method routinely used to characterise the phases present in crystalline materials from the position and relative intensity of the peaks found in XRD patterns [1]. The limited samples' preparation, non-destructive nature and fast experimental outputs are all general advantages of the technique. With respect to the characterisation of Ti alloys, the analysis of the XRD patterns of standards and experimental alloys indicates that XRD is able to detect and allow the identification of the phases present. The relative intensity of the XRD peaks detected is, normally, proportional to relative amount of the phase present in the microstructure of the alloy. However, the accuracy, as dictated by the minimum detection limit of the equipment, can lead to misjudgement of the phases present if not complemented with data from other characterisation' techniques, microstructural analysis in this instance. Microscopy techniques relevant to the clarification of the phases present in Ti alloys span from optical microscopy for determining the grain size in single-phase alloys [37], to SEM-EDS to confirm the chemistry and nature of generally μm-size phases [36], to TEM to commonly characterise nm-size features [38]. The need of complementing data for such verification constitutes a limitation of the XRD technique.

This study shows that XRD analysis is able to properly characterised Ti alloys composed by a single equilibrium phase, namely in the case of pure Ti (figure 1) and stable beta Ti alloys (figure 5). It is worth mentioning that the phases detected were analysed and matched with JCPDS No. 089–2762 (α-Ti) and JCPDS No. 044–1288 (β-Ti) cards. The space group and lattice parameter of the α-Ti phase are P63/mmc, and a = 2.9511 Å and c = 4.6843 Å, respectively. For the β-Ti phase, they are Im $\bar{3}$ m and a = 3.3065 Å. Only diffraction peaks of the equilibrium α-Ti and β-Ti phases were detected. The peak with the highest relative

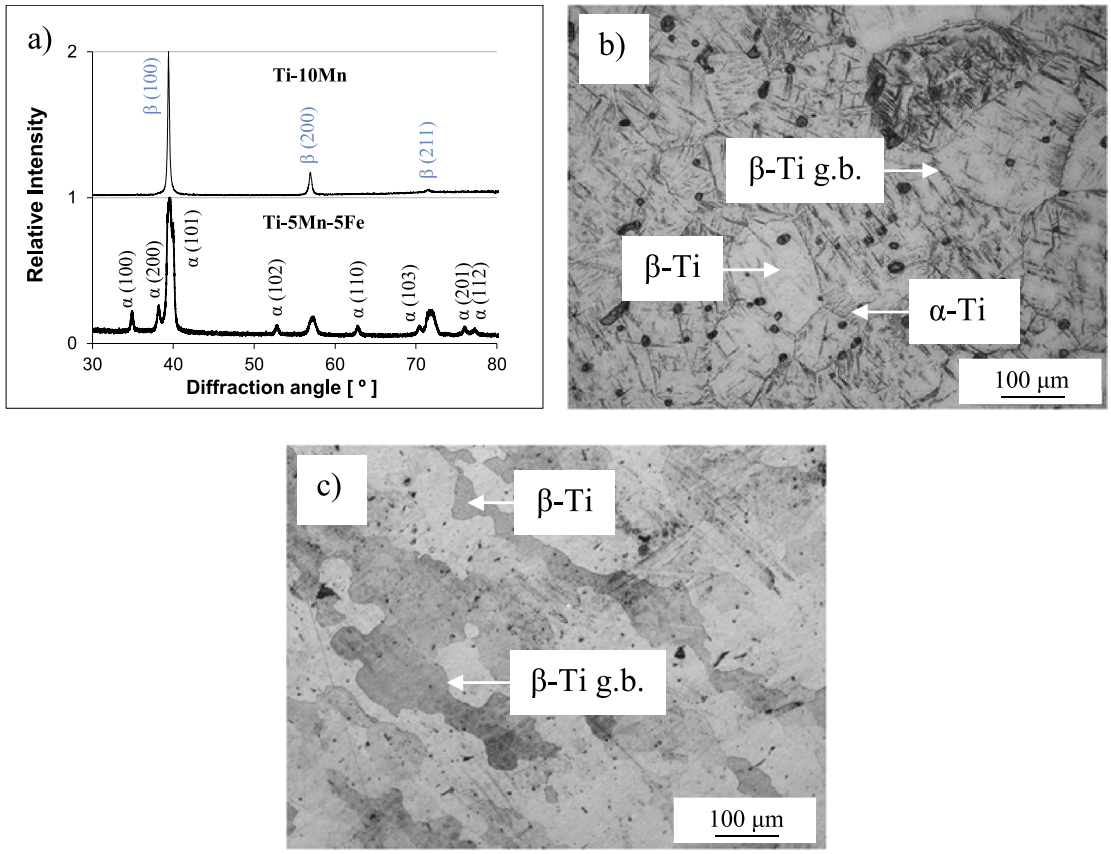

Figure 5. XRD patterns of the metastable/stable beta Ti alloys (a) and associated optical micrographs: (b) Ti-5Mn-5Fe (experimental), and (c) Ti-10Mn (experimental).

intensity is the α-Ti (101) plane in the case of pure Ti (figure 1(a)) and the β-Ti (100) family of planes for stable beta Ti alloys (figure 5(a)). This behaviour is common in literature as exemplified by the work of Niu *et al* [28] on Ti foils obtained via thermomechanical processing and that of Wang *et al* [36] on Ti-Mn-Nb alloys produced via arc melting, respectively.

Analysing biphasic Ti alloys, which include near-alpha (figure 2), alpha+beta (figure 3), near-beta (figure 4) and metastable beta (figure 5) Ti alloys, XRD analysis can successfully detect and identify the α-Ti and β-Ti phases, with the exception of near-alpha Ti alloys. When both phases are detected, the relative intensity of the diffraction peaks generally agrees with the relative amount of the two phases present in the microstructure. This is commonly encountered in experimental Ti alloys, as demonstrated by Qi *et al* [39] using a series of ternary Ti-6Zr-xFe (x = 4, 5, 6, 7%) alloys, as well as in conventional alloys such as Ti-13Nb-13Zr with respect to Ti-6Al-4V [40]. The relative amount of the α-Ti and β-Ti phases is also highly dependent on the manufacturing route as the intrinsic cooling rate significantly affects the resultant phases, and thus the actual peaks detected in the XRD pattern [34, 35].

As the relative intensity of the β-Ti phase' peaks increases that of the α-Ti phase' peaks decreases due to the higher amount of β-Ti phase stabilised in the alloy. This is commonly achieved by either increasing the content of β stabilisers or by using more potent β stabilisers. Accordingly, the greatest changes in relative intensity are visible from the α-Ti (101) plane for the α-Ti phase and from the β-Ti (100) family of planes for the β-Ti phase. For a sufficiently high amount of β stabilisers, which depends on their specific potency, the relative intensity of the β-Ti (100) family-planes' peak overcomes that of the α-Ti (101) plane' peak. This can be clearly seen by comparing the XRD pattens of figures 3 and 4. This is also discernible by comparing the near-beta Ti alloys (figure 4) where, in this case, the α-Ti (101) plane' diffraction peak is the strongest in the experimental Ti-5Mn-5Nb alloys but the β-Ti (100) family-planes' diffraction peak is the strongest in the standard Ti-5Al-5V-5Mo-3Cr alloy. This is in agreement with the resulting equilibrium microstructure where α-Ti phase grain boundaries are present in the former alloy whilst the β-Ti phase constitutes the grain boundaries of the latter alloy.

As previously mentioned, it is found that the only scenario where XRD analysis cannot successfully fully characterise Ti alloys is in the case of near-alpha alloys (figure 2). These type of Ti alloys normally bear a small amount of β stabilisers in their compositions, maximum 2%–3% by weight. This results in the stabilisation of small amount of β-Ti phase in the equilibrium microstructure (figure 2). Such amount is generally below the

Table 2. Values of the dimensionless *MoE* parameter of the Ti-based alloys analysed.

Composition	MoE_B (equation (1))	MoE_W (equation (2))	Alloy type
Pure Ti	0.0	0.0	—
Ti-3Al-2.5 V	−1.3	−1.3	—
Ti-1Cu-1Mn	1.1	1.8	β-rich
Ti-6Al-4V	−3.3	−3.8	—
Ti-2Nb-2Fe	6.4	4.4	Near-beta
Ti-5Al-5V-5Mo-3Cr	8.2	9.4	Near-beta
Ti-5Mn-5Nb	9.1	12.7	Near-beta / Beta
Ti-5Mn-5Fe	22.2	21.0	Beta
Ti-10Mn	15.4	22.6	Beta

detection limit of most XRD equipment found in research labs, and it is one of the primary limitations. This is confirmed by the study of Cai *et al* [41] where the main diffraction peaks of the β-Ti phase of the experimental Ti-9Al-1Mn and Ti-9Al-2Mn alloys was either not detected or barely visible as overlapping with one of the α-Ti phase peaks. Similarly, the β-Ti phase was not detected in the cast Ti-4Cu alloy in the study of Wang *et al* [42] or in the cast or hot isostatically pressed Ti-6.5Al-2Sn-3Zr-1.5Mo-1.5Nb-0.4Si-0.2Y-0.4 C alloy [29].

Ti alloys are generally classified as a function of the phases composing the material at room temperature after an annealing (i.e. slow cooling) heat treatment. The *MoE* parameter is commonly used to quantify the effect of the specific alloying elements on the stabilisation of the β-Ti phase so as to define the nature of the alloy. Furthermore, the *MoE* parameter is commonly used, along with other theoretical frameworks like the molecular orbital method [43], to design novel Ti alloys. Therefore, the establishment of a correlation between XRD results and the *MoE* parameter will provide an additional tool to verify the accuracy of the latter. This could result in the need of less experimental work for designing new optimised compositions. Equations (1) and (2) report the formula for the calculation of the dimensionless *MoE* parameter according to Bania [32] and Wang *et al* [33]:

$$MoE_B = Mo + 0.67\cdot V + 0.28\cdot Nb + 2.9\cdot Fe + 1.6\cdot Cr + 0.77\cdot Cu + 1.54\cdot Mn - Al \quad (1)$$

$$MoE_W = Mo + 1.25\cdot V + 0.28\cdot Nb + 1.93\cdot Fe + 1.84\cdot Cr + 1.5\cdot Cu + 2.26\cdot Mn - 1.47\cdot Al \quad (2)$$

As a general rule, alloys with $0 \leqslant MoE < 5$ are β-rich, alloys with $5 \leqslant MoE < 10$ are near-beta, and alloys with $MoE \geqslant 10$ are β [44]. Table 2 shows the values of the *MoE* parameter as calculated via equations (1) and (2) for the alloys analysed where it can be seen that there is a good agreement between the two, with the exception of the Ti-5Mn-5Nb alloy which has a different classification depending on the equation used. Moreover, it is worth noting the inconsistency for many of the alloys with the classification of table 1.

Prediction of physical properties like thermal conductivity and electrical resistivity is generally done in literature using structural-analytical models. This is because they are rapid, physically based, reasonably accurate tools when the microstructure is uncertain [45]. The five most common structural-analytical models are the parallel model (P), the Maxwell-Eucken 1 model (ME1), the effective medium theory (EMT), the Maxwell-Eucken 2 model (ME2), and the series model (S). The variation of a relative property with a phase's volume fraction, and the associated physical structures as insets, for each structural-analytical model are shown in figure 6(a)). The models were tested to estimate the variation of the β-Ti phase volume fraction with the addition of the alloying elements accounted for using the *MoE* parameter (figure 6(b)). This was done comparing it with the experimental data obtained from the analysis of the respective XRD patterns (figures 1–5). The mean squared error of each prediction was calculated to estimate their accuracy and the results are shown in figure 6(c)). It can be seen that the reliability of the prediction progressively worsens from the P to the S model. The P model, which is equivalent to the rule of mixtures, is the most precise to estimate the amount of β-Ti phase as a function of the *MoE* parameter. Furthermore, a slightly better prediction is obtained if the latter is calculated using equation (2) rather than equation (1).

4.1. Comment on the characterisation of metastable phases

As point out in the introduction, different combinations of alloying elements and processing conditions might lead to the formation of the martensitic α' and α'' phases, or the athermal/isothermal ω phase [14]. Identification and quantification of the martensitic phases purely based on XRD patterns can be challenging as their peaks mostly overlap with those of the equilibrium α-Ti phase. Analysis of minor variations of the diffraction angle and peaks' width can be combined with the output of other characterisation techniques to discern them. A clear example where the diffraction peaks of the α/α' peaks overlap in the XRD pattern is the

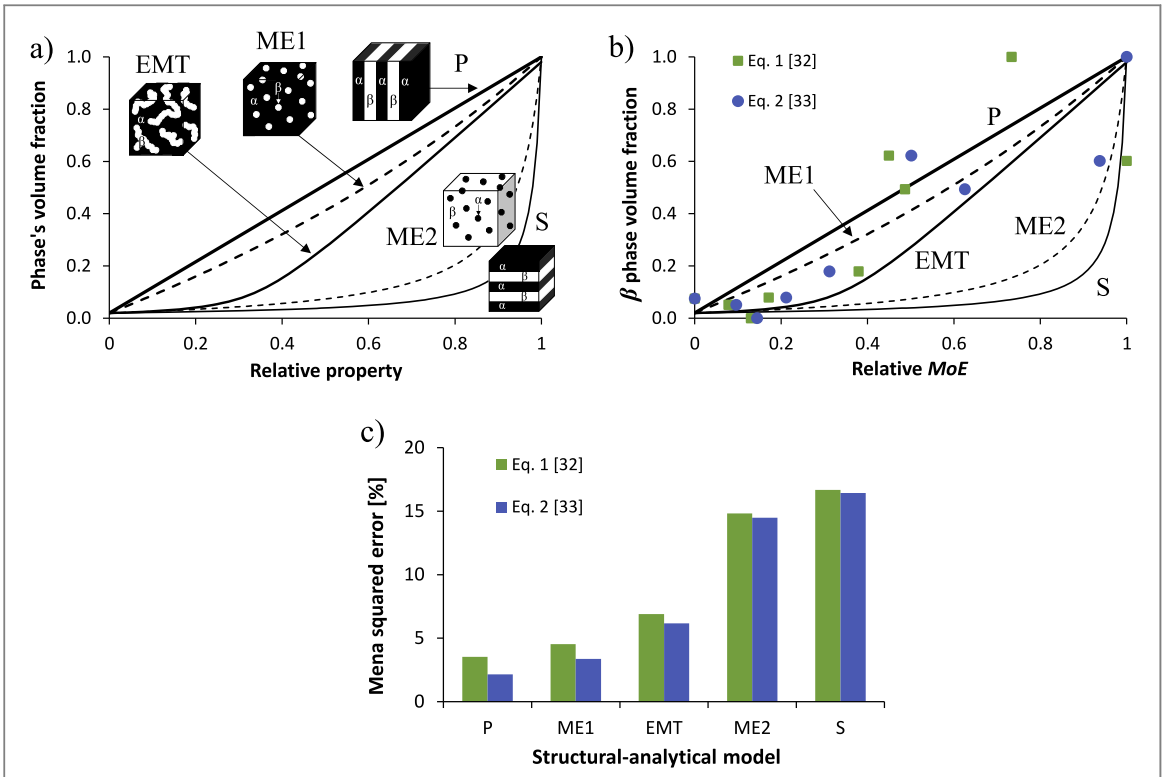

Figure 6. Prediction of a relative property with a phase's volume fraction using structural-analytical model (a), prediction of the β-Ti phase volume fraction versus relative *MoE* values with superimposed experimental data (b), and mean squared error of the structural-analytical models (c). Legend: P (Parallel Model), ME1 (Maxwell-Eucken 1), EMT (Effective Medium Theory), ME2 (Maxwell-Eucken 2), and S (Series Model).

study of Sun at el. [46] on the martensitic Ti-6Al-4V alloy. Because of its derivation from the equilibrium β-Ti phase, identification of the metastable ω phase can also be difficult especially if its volume fraction and size are low. This is demonstrated by the work of Tang *et al* [17] on metastable β titanium alloys where TEM was needed to properly identify and characterise the ω phase. There are however some instances, like in the case of the spinodal decomposition of the quenched β-Ti phase, where identification of the metastable ω phase can be achieved as the $\beta(200)$ diffraction peak splits into two overlapping peaks, one related to β-Ti and the other to ω, as the decomposition progresses [47].

5. Conclusions

This work considered the benefits and limitations of using x-ray diffraction (XRD) for the identification of the phases present in different types of Ti-based alloys characterised by equilibrium microstructure. From the analysis of the respective XRD patterns, it is confirmed that XRD is a simple and powerful technique to gain insight on the crystallinity, structure, and relative amount of the phases present in Ti-based alloys. For instance, XRD analysis can properly fully characterised Ti alloys composed by a single equilibrium phase such as in alpha and beta Ti alloys. This is significant as XRD can be used as a fast non-destructive screening technique in industrial applications. Additionally, the technique is reliable for most of the other types of Ti alloys, with the clear exception of near-alpha alloys. It is however advisable, and it is sometime actually required, to complement the characterisation of the alloys by means of other techniques, the simplest option being microscopy, to fully characterise the structure of the material. Correlation of the output of XRD analysis with the molybdenum equivalent parameter (*MoE*) that takes into account the stabilisation strength of different alloying elements yields good consistency. The parallel structural-analytical model can be used to reliably predict the β-Ti phase volume fraction as a function of *MoE*.

Acknowledgments

This research did not receive any specific grant from funding agencies in the public, commercial, or not-for-profit sectors.

Data availability statement

The authors declare that the data supporting the findings of this study are available within the paper. The data that support the findings of this study are available upon reasonable request from the authors.

ORCID iDs

L Bolzoni https://orcid.org/0000-0003-2589-9449

References

[1] Bunaciu A A, Udriştioiu E G and Aboul-Enein H Y 2015 X-ray diffraction: instrumentation and applications *Crit. Rev. Anal. Chem.* **45** 289–99
[2] Zhou X, Fang H, Yuan T and Li R 2023 Effect of slight sn modification on mechanical properties and corrosion behavior of Ti- (2-4 wt%) Mn alloys fabricated via powder metallurgy *Mater. Charact.* **203** 113068
[3] Bian X, Heller L, Kadeřávek L and Šittner P 2022 In-situ synchrotron x-ray diffraction texture analysis of tensile deformation of nanocrystalline NiTi wire in martensite state *Applied Materials Today* **26** 101378
[4] Dolabella S, Borzì A, Dommann A and Neels A 2022 Lattice strain and defects analysis in nanostructured semiconductor materials and devices by high-resolution x-ray diffraction: theoretical and practical aspects *Small Methods* **6** 2100932
[5] Muhammed Shafi P and Chandra Bose A 2015 Impact of crystalline defects and size on x-ray line broadening: a phenomenological approach for tetragonal SnO_2 nanocrystals *AIP Adv.* **5** 057137
[6] Kaduk J A, Billinge S J L, Dinnebier R E, Henderson N, Madsen I, Černý R, Leoni M, Lutterotti L, Thakral S and Chateigner D 2021 Powder diffraction *Nat. Rev. Methods Primers* **1** 77
[7] Geetha M, Singh A K, Asokamani R and Gogia A K 2009 Ti based biomaterials, the ultimate choice for orthopaedic implants - a review *Prog. Mater. Sci.* **54** 397–425
[8] Niinomi M 2008 Mechanical biocompatibilities of titanium alloys for biomedical applications *J. Mech. Behav. Biomed. Mater.* **1** 30–42
[9] Niinomi M 1998 Mechanical properties of biomedical titanium alloys *Mater. Sci. Eng.* A **243** 231–6
[10] Boyer R, Welsch G and Collings E W 1998 *Materials Properties Handbook: Titanium Alloys* (A. International)
[11] Yang F, Gabbitas B, Dore M, Ogereau A, Raynova S and Bolzoni L 2018 On microstructural evolution and mechanical properties of Ti-5Al-5V-5Mo-3Cr alloy synthesised from elemental powder mixtures *Mater. Chem. Phys.* **211** 406–13
[12] Wang H, Fang Z Z and Sun P 2010 A critical review of mechanical properties of powder metallurgy titanium *Int. J. Powder Metall.* **46** 45–57
[13] Kumar P and Chandran K S R 2017 Strength-ductility property maps of powder metallurgy (PM) Ti-6Al-4V alloy: a critical review of processing-structure-property relationships *Metallurgical and Materials Transactions* A **48** 2301–19
[14] Banerjee D and Williams J C 2013 Perspectives on titanium science and technology *Acta Mater.* **61** 844–79
[15] Santos P F, Niinomi M, Liu H, Cho K, Nakai M, Itoh Y, Narushima T and Ikeda M 2016 Fabrication of low-cost beta-type Ti-Mn alloys for biomedical applications by metal injection molding process and their mechanical properties *J. Mech. Behav. Biomed. Mater.* **59** 497–507
[16] Romero C, Yang F, Zhang S and Bolzoni L 2020 Effect of thermomechanical microstructural modification and resulting crystallographic texture on the crack initiation mechanism and fatigue behaviour of PM Ti-6Al-4V *Mater. Sci. Eng.* A **792** 139836
[17] Tang B, Chu Y, Zhang M, Meng C, Fan J, Kou H and Li J 2020 The ω phase transformation during the low temperature aging and low rate heating process of metastable β titanium alloys *Mater. Chem. Phys.* **239** 122125
[18] Raganya L, Moshokoa N, Obadele B, Makhatha E and Machaka R 2021 Microstructure and mechanical properties of Ti-Mo-Nb alloys designed using the cluster-plus-glue-atom model for orthopedic applications *Int. J. Adv. Manuf. Technol.* **115** 3053–64
[19] Bolzoni L, Ruiz-Navas E M and Gordo E 2014 Powder metallurgy CP-Ti performances: hydride-dehydride versus sponge *Mater. Des.* **60** 226–32
[20] Bolzoni L, Ruiz-Navas E M and Gordo E 2013 Influence of sintering parameters on the properties of powder metallurgy Ti-3Al-2.5V alloy *Mater. Charact.* **84** 48–57
[21] Bolzoni L, Alqattan M, Peters L, Alshammari Y and Yang F 2020 Ternary Ti alloys functionalised with antibacterial activity *Sci. Rep.* **10** 22201
[22] Bolzoni L, Esteban P G, Ruiz-Navas E M and Gordo E 2012 Mechanical behaviour of pressed and sintered titanium alloys obtained from prealloyed and blended elemental powders *J. Mech. Behav. Biomed. Mater.* **14** 29–38
[23] Bolzoni L, Paul M and Yang F 2022 Effect of combined lean additions of isomorphous and eutectoid beta stabilisers on the properties of titanium *Journal of Materials Research and Technology* **21** 3828–43
[24] Raynova S, Imam M A, Yang F and Bolzoni L 2019 Hybrid microwave sintering of blended elemental Ti alloys *J. Manuf. Processes* **39** 52–7
[25] Paul M, Alshammari Y, Yang F and Bolzoni L 2023 New ternary powder metallurgy Ti alloys via eutectoid and isomorphous beta stabilisers additions *Sci. Rep.* **13** 1150
[26] Bolzoni L, Paul M, Yang F and Alshammari Y 2023 Titanium alloys developed on the basis of the addition of cheap strong eutectoid β-stabilisers *J. Mater. Sci.* **58** 5037–47
[27] Alshammari Y, Yang F and Bolzoni L 2019 Mechanical properties and microstructure of Ti-Mn alloys produced via powder metallurgy for biomedical applications *J. Mech. Behav. Biomed. Mater.* **91** 391–7
[28] Niu L *et al* 2017 Mechanical behavior and deformation mechanism of commercial pure titanium foils *Mater. Sci. Eng.*A **707** 435–42
[29] Yu Y, Cai Y H, Chen X H, Wang T, Wu Y D, Si J J, Hui X D and High A 2016 Strength and elastic carbon containing near-α Ti alloy prepared by hot isostatic pressing process *Mater. Sci. Eng.* A **651** 961–7
[30] Bolzoni L, Ruiz-Navas E M and Gordo E 2012 Influence of vacuum hot-pressing temperature on the microstructure and mechanical properties of Ti-3Al-2.5V alloy obtained by blended elemental and master alloy addition powders *Mater. Chem. Phys.* **137** 608–16
[31] Molchanova K 1965 *Phase Diagrams of Titanium Alloys* (Jerusalem: Israel Program for Scientific Translations) p. 154 Translation of atlas diagram Sostoyaniya Titanovyk Splavov, Israel program for scientific translations
[32] Bania P J 1994 Beta titanium alloys and their role in the titanium industry *JOM* **46** 16–9

[33] Wang Q, Dong C and Liaw P K 2015 Structural stabilities of β-Ti alloys studied using a new mo equivalent derived from [$\beta/(\alpha+\beta)$] phase-boundary slopes *Metallurgical and Materials Transactions* A **46** 3440–7
[34] Luo Y, Xie Y, Zhang Z, Liang J and Zhang D 2023 Improving strain hardening capacity of high-strength Ti-6Al-4V alloy by a dual harmonic structure *Journal of Materials Research and Technology* **26** 1122–35
[35] Schwab H, Palm F, Kühn U and Eckert J 2016 Microstructure and mechanical properties of the near-beta titanium alloy Ti-5553 processed by selective laser melting *Mater. Des.* **105** 75–80
[36] Zhang H, Wang C, Pyczak F, Ebel T and Liu X 2023 A new kind of biomedical Ti-Mn-Nb alloy *Physica Status Solidi (a)* **220** 2200348
[37] Chen H, Yao Y, Warner J A, Qu J, Yun F, Ye Z, Ringer S P and Zheng R 2017 Grain size quantification by optical microscopy electron backscatter diffraction and magnetic force microscopy *Micron* **101** 41–7
[38] Zhang B, Wu X and Zhang D 2023 Hierarchical microstructure and strain partition of a PM $\alpha+\beta$ titanium alloy with an ultrahigh strength-ductility synergy *Mater. Charact.* **199** 112835
[39] Qi P, Li B, Wang T, Zhou L and Nie Z 2021 Microstructure and properties of a novel ternary Ti-6Zr-xFe alloy for biomedical applications *J. Alloys Compd.* **854** 157119
[40] Hacisalihoglu I, Samancioglu A, Yildiz F, Purcek G and Alsaran A 2015 Tribocorrosion properties of different type titanium alloys in simulated body fluid *Wear* **332-333** 679–86
[41] Cai Q, Xu C, Chen X, Xi W, Cheng J, Chen Z and Chen J 2023 Effect of Mn and Mo on the microstructure and electrical resistivity of Ti-Al alloy prepared by mechanical alloying and spark plasma sintering *J. Alloys Compd.* **947** 169608
[42] Wang Z, Fu B, Wang Y, Dong T, Li J, Li G, Zhao X, Liu J and Zhang G 2022 Effect of Cu content on the precipitation behaviors mechanical and corrosion properties of As-Cast Ti-Cu alloys *Materials* **15** 1696
[43] Morinaga M 2016 Alloy design based on molecular orbital method *Mater. Trans.* **57** 213–26
[44] Cotton J D, Briggs R D, Boyer R R, Tamirisakandala S, Russo P, Shchetnikov N and Fanning J C 2015 State of the art in beta titanium alloys for airframe applications *JOM* **67** 1281–303
[45] Bolzoni L, Carson J K and Yang F 2021 Combinatorial structural-analytical models for the prediction of the mechanical behaviour of isotropic porous pure *Metals Acta Materalia.* **207** 116664
[46] Sun S, Zhang D, Palanisamy S, Liu Q and Dargusch M S 2022 Mechanical properties and deformation mechanisms of martensitic Ti6Al4V alloy processed by laser powder bed fusion and water quenching *Mater. Sci. Eng.* A **839** 142817
[47] Romero C, Raynova S, Yang F and Bolzoni L 2018 Ultrafine microstructures in eutectoid element bearing low-cost Ti-Fe alloys enabled by slow bainite formation *J. Alloys Compd.* **769** 226–32